PROTEINS: Structure, Function, and Bioinformatics 64:863–873 (2006)

# Molecular Dynamics Simulations of the Hydrophobin SC3 at a Hydrophobic/Hydrophilic Interface

**Hao Fan,[1] Xiaoqin Wang,[2] Jiang Zhu,[3] George T. Robillard,[2] and Alan E. Mark[1,4]***

[1]*Groningen Biomolecular Sciences and Biotechnology Institute (GBB), Department of Biophysical Chemistry, University of Groningen, Groningen, the Netherlands*

[2]*BioMaDe Technology, Groningen, the Netherlands*

[3]*Department of Biochemistry and Molecular Biophysics, Columbia University, Howard Hughes Medical Institute, New York, New York*

[4]*School of Molecular and Microbial Sciences, University of Queensland, Queensland, Australia*

***ABSTRACT*** **Hydrophobins are small (~100 aa) proteins that have an important role in the growth and development of mycelial fungi. They are surface active and, after secretion by the fungi, self-assemble into amphipathic membranes at hydrophobic/hydrophilic interfaces, reversing the hydrophobicity of the surface. In this study, molecular dynamics simulation techniques have been used to model the process by which a specific class I hydrophobin, SC3, binds to a range of hydrophobic/hydrophilic interfaces. The structure of SC3 used in this investigation was modeled based on the crystal structure of the class II hydrophobin HFBII using the assumption that the disulfide pairings of the eight conserved cysteine residues are maintained. The proposed model for SC3 in aqueous solution is compact and globular containing primarily β-strand and coil structures. The behavior of this model of SC3 was investigated at an air/water, an oil/water, and a hydrophobic solid/water interface. It was found that SC3 preferentially binds to the interfaces via the loop region between the third and fourth cysteine residues and that binding is associated with an increase in α-helix formation in qualitative agreement with experiment. Based on a combination of the available experiment data and the current simulation studies, we propose a possible model for SC3 self-assembly on a hydrophobic solid/water interface. Proteins 2006;64:863–873.**



**Key words: hydrophobin; trSC3; interface; structure prediction; molecular dynamics**

## INTRODUCTION

Hydrophobins are a family of small proteins that appear unique to mycelial fungi. They are found in a water-insoluble form on the surfaces of different fungal structures, such as aerial hyphae, spores, and fruiting bodies.[1–3] Hydrophobins are surface active and are able to self-assemble into an amphipathic membrane at hydrophobic/hydrophilic interfaces, thereby reversing the hydrophobicity of the surface.[4–10] Not only does this make hydrophobins interesting from a biological perspective but also suggests a wide variety of medical and industrial applications.[1,11–16]

Many genes coding for hydrophobins have been identified. The different hydrophobins identified to date show only limited sequence identity. For example, between the three hydrophobins of *Schizophyllum commune*, SC3, SC4, and SC1, the sequence identity is only 39%. This decreases to 11% if another two hydrophobins, RODA and EAS, are considered simultaneously.[1,17] Despite the variations in sequence, all known hydrophobins have eight cysteine residues, the spacing between which is conserved and which are believed to form four intramolecular disulfide bridges.[18,19] Hydrophobins can be classified into two classes based on differences in their hydropathy patterns and the solubility of the assembled membranes.[17] Class I hydrophobins form insoluble membranes with rodlet structures on the hydrophobic side of the assembled membranes.[5,6,9,10,19,20] Class II hydrophobins do not display rodlet structures and the assembled protein membranes are less stable.[7,21]

SC3, secreted by *S. commune*, is the best characterized of the class I hydrophobins. It is involved in the formation of aerial hyphae and in the attachment of hyphae to hydrophobic interfaces.[3,6] Fluorescence resonance energy transfer (FRET) measurements indicate that SC3 is primarily dimeric in solution.[22,23] When the soluble form of SC3 is exposed to a hydrophobic surface, an increase in α-helical content is observed both by circular dichroism spectroscopy and by fluorescence measurements.[22,24] FRET experiments indicate that upon binding to Teflon, SC3 dimers dissociate, adopt the α-helical state, and become immobilized.[22,23] The α-helical state is stable on Teflon (>10 h). At an air/water interface, the α-helical state rapidly converts to a stable assembly consisting primarily of β-sheet.[22,24,25] SC3 has also been shown to self-assemble at an oil/water interface.[26]

*Correspondence to: Alan E. Mark, Groningen Biomolecular Sciences and Biotechnology Institute (GBB), Department of Biophysical Chemistry, University of Groningen, Nijenborgh 4, 9747 AG Groningen, the Netherlands. E-mail: a.mark@uq.edu.au

Received 23 October 2005; Revised 27 December 2005; Accepted 5 January 2006

Published online 12 June 2006 in Wiley InterScience (www.interscience.wiley.com). DOI: 10.1002/prot.20936

To determine the region of the protein responsible for binding to specific surfaces, fragments of SC3 have also been studied. Performic acid-oxidized SC3 (PFA-SC3) has been specifically digested by endoproteinase Asp-N at the sites of the eight cysteine residues and the aspartic acid in the loop between the third and fourth cysteine. Matrix-assisted laser-desorption/ionization–time-of-flight measurements have been used to identify two peptide fragments that have high affinity for Teflon. The peptides are Cys39–Ser63 and Asp64–Ser72, corresponding to the first and second half of the loop between the third and fourth cysteines. The circular dichroism spectrum of the peptides bound to Teflon suggests the formation of an α-helical state. When PFA-SC3 is bound to Teflon, the region Cys39–Ser63 has been found to be highly protected from hydrogen/deuterium exchange, indicating a low solvent accessibility. Together, these data suggest that the loop region between the third and fourth cysteines is responsible for both binding and the transition to the α-helical state.[27]

Mature SC3 has 31 amino acids preceding the first cysteine residue and contains 16–22 mannose residues attached to the 12 threonine residues in this region.[24] The deletion of 25 of the 31 residues at the N-terminus of SC3 also results in the removal of all mannose residues. This has been reported to have no effect on either the self-assembly or the changes in secondary structure observed on binding to hydrophobic surfaces. The deletion does, however, change the physiochemical properties of the hydrophilic side of the assembled membrane.[13] When N-terminal truncated SC3 (trSC3) is expressed in the fungus *S. commune*, posttranslational modification results in one glycine at the N-terminus frequently being removed, leading to the presence of two peaks in mass spectra. However, the two protein species (with and without the N-terminal Gly) behave in a similar manner at interfaces both in terms of self-assembly and changes in secondary structure (data not published).

A major factor limiting the further understanding of the binding and assembly of SC3 at interfaces is the lack of a detailed, three-dimensional structure. Attempts have been made to use molecular dynamics (MD) simulations to study the folding of the trSC3 (without the N-terminal Gly) in solution and at a hexane/water interface.[28] In that work, the disulfide pairing indicated in Figure 1(a) was used to constrain the structure of the protein.[18] This disulfide pattern, which had been inferred from early experimental data, was widely accepted to be correct at that time. The simulations performed using this disulfide bridging pattern (i.e., Cys 1 to 2, 3 to 4, 5 to 6, and 7 to 8) suggested that trSC3 at a hexane/water interface underwent a rapid disorder-to-order folding transition leading to an elongated planar structure with extensive β-sheet content.

Recently, the first three-dimensional structure of a hydrophobin, that of HFBII, a class II hydrophobin from *Trichoderma reesei*, was determined at 1.0 Å resolution using X-ray crystallography.[29] The structure is a symmetric dimer with the two monomers packing against each other via a hydrophobic patch. The monomer is a compact single domain protein with a novel fold. Most importantly, the disulfide pattern that had been suggested previously was not observed [Fig. 1(b)]. Although the overall sequence identity between class I and class II hydrophobins is weak, the disulfide pattern and spacing are conserved.[17] Therefore, it is highly likely that the disulfide pairing in class I hydrophobins, such as SC3, will be the same as that found in HFBII.

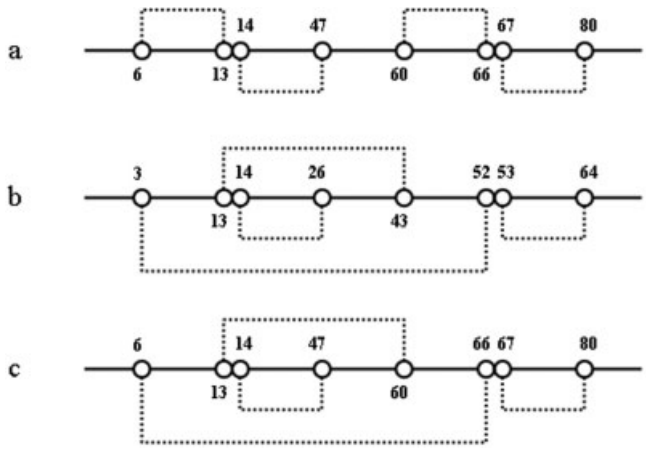


Fig. 1. **a:** The pattern of disulfide bridges in hydrophobins proposed previously. **b:** The disulfide bridges in hydrophobin HFBII found experimentally. **c:** The current proposed disulfide bridges in hydrophobin trSC3.

In the current study, we use the structure of HFBII to propose a three-dimensional model of trSC3 (without the N-terminal Gly) incorporating the disulfide bridge pattern found in HFBII as constraints. This model for trSC3 was subjected to extensive MD simulations in water to refine the structure. We then investigated the behavior of two alternative conformations of trSC3 monomer at different hydrophobic/hydrophilic interfaces in order to shed light on early events during binding and self-assembly. Finally, a 23-residue fragment corresponding to the region Asn41–Ser63 in SC3 was studied. Simulations performed on this peptide were used to investigate the difference in behavior of a monomer and a dimer at various interfaces.

## MATERIALS AND METHODS

### trSC3 Structure Prediction

trSC3 is composed of 86 amino acids. Starting from the sequence of native SC3, the 29 N-terminal residues were removed and substituted by the sequence Gly-His-Pro, which is found in many hydrophobins at this position. The structure prediction protocol consisted of three steps: sequence alignment, model building, and structure refinement. First, the sequence of trSC3 was submitted to the SPARKS server (http://phyyz4.med.buffalo.edu/hzhou/anonymous-fold-sparks2.html) to determine the optimal template for model building. SPARKS is a fold recognition method based on the combination of a profile–profile sequence alignment and an elaborate threading function.[30] The top 10 matches were ranked according to their significance score (Z-score). Despite its low sequence iden-

tity, HFBII [Protein Data Bank (PDB) ID: 1r2m] is the second best match for trSC3 among all available structures and the best match among the available hydrophobins.[29] The best match using the SPARKS server was with pancreatic lipase (PDB ID: 1lpb); however, because this protein does not contain equivalent cysteine residues, it was not considered a suitable target. One monomer (chain A) from the dimeric structure of HFBII was used as the template to build alternative models for trSC3. A total of 10 models were built using the program *nest* with different random number generator seeds. *nest* is a recently developed homology modeling program based on a rigid-body assembly of structural elements with loops modeled using an artificial evolution algorithm.[31] The default parameters were applied. The 10 models were then refined using the TINKER package.[32] An all-atom OPLS-AA force field[33–37] was used together with the mAGB implicit solvent model.[38,39] The 10 structures were subjected to energy minimization using the LBFGS quasi-Newton nonlinear optimization algorithm.[40]

### MD Simulations

All simulations were performed in explicit solvent using the GROMACS (Groningen Machine for Chemical Simulation) package[41–43] in conjunction with the GROMOS96 43a2 force field.[44,45] The simulations were performed at constant volume in a periodic rectangular box. To evaluate the nonbonded interactions, a twin-range cut-off of 0.9 and 1.4 nm was used. To minimize the effects of truncating the electrostatic interactions beyond the 1.4-nm long-range cut-off, a reaction field correction was applied using a relative dielectric constant of 78.[46] Explicit hydrogen atoms in the force field were replaced by dummy interaction sites, the positions of which were constructed each step from the coordinates of the heavy atoms to which they are attached. This allows a time step of 4 fs to be used without affecting the thermodynamic properties of the system significantly.[47] Covalent bonds in the protein were constrained using the LINCS algorithm.[48] The SETTLE algorithm was used to constrain the geometry of the water molecules.[49,50] During the simulations, the temperature was maintained at 300 K by coupling to an external heat bath with a relaxation time of 0.1 ps.[51] The protonation state of ionizable groups in each of the proteins was set appropriate for pH 7.0. No counter-ions were added to neutralize the system. We note in this regard that at pH 7.0 there are only four charged residues on the protein and the net charge is only −2. Statistically, counter-ions would only rarely be found within the box volume simulated (at realistic protein concentrations). A cubic box with an edge length of 5.3 nm was used in the reference simulations so that a minimum distance of 1.0 nm was always maintained between the protein and the edge of the unit cell.

### Interface Simulations

#### *trSC3 model*

To obtain the starting configuration for the simulations at the different interfaces, one dimension of the box used in the 400-ns simulation was increased to accommodate the hydrophobic phase. For the air/water system, the *z*-axis of the initial cubic box was extended by 3.0 nm. The volume of the new cell, which in part contained vacuum, was then held constant during the simulations. The trSC3 molecule (SCI or SCII) was initially restrained at the center of water phase until the system had equilibrated. An identical procedure was used to generate the oil/water interface except that the oil phase consisted of dodecane molecules which are liquid at 300 K. For the hydrophobic solid/water interface, a solid surface was mimicked by a hydrocarbon lattice composed of seven planes of cyclohexane-like molecules. The molecules in the "chair" conformation shared the same orientation and were aligned side by side on each plane. Such a plane was then duplicated seven times to form a hydrophobic lattice 1.4 nm thick, with a distance of 0.2 nm between every two adjacent planes. The lattice was placed at one side of the water phase. The box was extended by 1.4 nm in this direction. The lattice remained static in the simulations. The oil/water and the solid/water interfaces were also simulated at constant volume after 10 ps of equilibration at 1 bar with position restraints on the protein.[51]

#### *Fragment Asn15–Ser37*

A 23-residue peptide fragment corresponding to residues Asn15 to Ser37 in the first half of the 14–47 loop in trSC3 was extracted from the homology model. Starting from this coiled structure, two 100-ns simulations in aqueous solution were then performed. The final configurations, termed LPa and LPb, were used for further studies. Three simulations of 200 ns each were then performed in water: one of the configuration LPa, one of the configuration LPb, and another of a system containing both LPa and LPb. In this system, LPa and LPb were placed initially in a random orientation with a minimum distance of 1.0 nm between the two peptides. The rapid ($<$1 ns) formation of a peptide dimer (termed LPa/LPb) was observed. The structure at 100 ns, termed LPab, was taken to represent a possible dimeric state of the peptide. LPa, LPb, LPa/LPb, and LPab were then used as starting configurations in a series of simulations at different interfaces. The two interfaces, air/water and hydrophobic solid/water were prepared as for the trSC3 model.

## RESULTS

### Structure Prediction

Based on sequence and structural information, the structure of HFBII (PDBID 1r2m) was identified as one of the top matches to the N-terminal trSC3 by the SPARKS server.[29,30] The sequence alignment is shown in Figure 2, along with the secondary structure assignment for 1r2m obtained using the DSSP criteria and the secondary structure predicted for trSC3 using PSIPRED.[52–54] Although the sequence identity between trSC3 and HFBII is only 17%, the SPARKS server did align the cysteine residues in the two sequences, supporting the proposal that the disulfide bonding pattern is conserved between class I and class II hydrophobins. Two large insertions in the trSC3 sequence (13 and 8 residues, respectively) between the third


Fig. 2. The sequence alignment between the A chain of class II hydrophobin HFBII (PDB ID: 1r2m) and the class I hydrophobin trSC3, together with the secondary structure assignment for 1r2m and the secondary structure predicted for trSC3. [Color figure can be viewed in the online issue, which is available at www.interscience.wiley.com.]

and fourth cysteines resulted in a much larger loop than that found in HFBII. A small part of this loop (Thr26-Leu29) in trSC3 was predicted to form a helical structure. In contrast, in HFBII, a 10-residue region around the fifth cysteine, which contains several hydrophilic residues, was found to be helical. The first monomer (chain A) of HFBII was used as a template to construct 10 candidate homology models for trSC3 all of which shared the same fold motif. After energy minimization, the best model was selected considering both the total energy of the system and whether critical structural features were maintained (e.g., the overall fold and disulfide pairings, as determined by visual inspection). This model contained a small region of β-sheet that formed during energy minimization. The cysteine bridges 14–47 and 67–80 are exposed at the protein surface, connected by sequential cysteine residues (i.e., the third and fourth Cys as well as the seventh and eighth Cys). The other two linkages, 6–66 and 13–60 are buried inside the structure, providing a connection between the N- and C-termini of the protein. Figure 3 shows a superposition of the initial model of trSC3 and the structure of the HFBII monomer used as a template. Note that the disulfide bridges in both the model and the template structure nearly coincide. In addition, the loop region between the third and fourth Cys in trSC3 locates closely to the corresponding region in HFBII. In HFBII, this region is involved in the formation of a hydrophobic patch which lies at the dimer interface and is believed to be important for the function of the protein.[29]

### SC3 Model in Aqueous Solution

Although SC3 exists primarily as a dimer in solution, the dimer is in rapid equilibrium with monomeric SC3. The monomer is believed to be the surface active form and thus it is the behavior of the monomeric, water-soluble state of trSC3 that is of interest.[23] The template used to predict the structure of trSC3 was taken from the HFBII dimer. Thus, the initial trSC3 model could potentially incorporate some characteristics of the oligomer. To refine the structure, the initial model of monomeric trSC3 was subjected to a 400-ns MD simulation in explicit water. Figure 4 shows the positional root-mean-square deviation (RMSD) of all backbone atoms as a function of simulation time after a least-square best fit to two alternative structures obtained from the simulation at 100 and 300 ns (SCI and SCII). As can be seen in Figure 4, large deviations are observed in the first 100 ns in both cases, indicating significant changes in the model with respect to the two reference structures. The changes in RMSD over the subsequent 300 ns with respect to SCI or SCII are relatively minor. The secondary structure content calculated using the DSSP algorithm shows some variation in β-sheet content during the first 100 ns, which stabilizes thereafter (Fig. 5). The changes in RMSD and secondary structure content suggest that, after 100 ns, the system adopts a relatively stable conformation. Overall, the structural differences between SCI and SCII are small. The backbone RMSD between the two structures is 0.25 nm. However, excluding the region between the third and the fourth Cys, which is quite flexible, the RMSD between SCI and SCII decreases to only 0.14 nm. Both structures contain 4 β-hairpins [Fig. 6(a,b)]. The N-terminal region (residues 5–8) forms a plane with the β-hairpin of residues 50–59 stabilized by two disulfide bridges 6–66 and 13–60. Another β-sheet is formed near the C-terminus incorporating residues Glu68 to Ile78 which are associated with the disulfide bridge 67–80. The loop 14–47 is located on the other side of the structure, extending away from N- and C-termini. The β-sheet content of this loop increases after the first 100 ns. Two β-hairpins are evident in this region in both SCI and SCII. One involves residues 15–24, the other involves residues 35–45 and forms in the same plane as the hairpin 68–78. In the 400-ns reference simulation, some helix formation was observed but only in the loop 14–47 and primarily in the period from 240 to 340 ns. The electrostatic potential of SCI was calculated at neutral pH and physiological salt concentration.[55] The potential mapped onto the contact surface of the molecule[56] is shown in Figure 6(c). As can be seen, regions of high electrostatic potential are only found on the side of the SCI surface where the two termini are located. The trSC3 model in solution is thus relatively hydrophilic on this side but hydrophobic on the side containing the loop 14–47, a feature proposed previously by Joel Mackay and coworkers in relation to the "easily wetable" class I hydrophobin EAS (personal communication).

SCI and SCII were selected to represent alternative folds of trSC3 in solution and used to initiate further studies of this protein. At each type of interface, two identical simulations of 100-ns length were performed and the results compared. One simulation was initiated from the SCI structure. The other was initiated from the SCII structure.

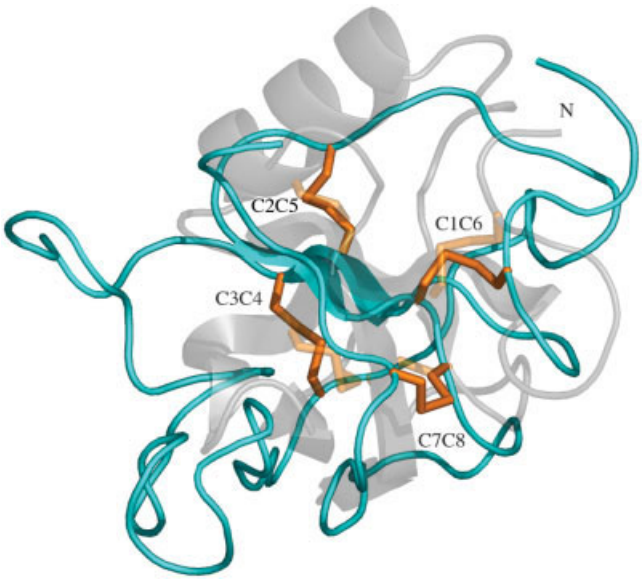


Fig. 3. The predicted structure of trSC3 (solid) superimposed on the crystal structure of HFBII monomer (partially transparent). Both structures have similar folds and an identical network of disulfide bridges (orange). The disulfide bridges are Cys1–Cys6, Cys2–Cys5, Cys3–Cys4, and Cys7–Cys8 corresponding to the bridges connected by the first and sixth Cys, the second and fifth Cys, the third and fourth Cys, and the seventh and eighth Cys, respectively.

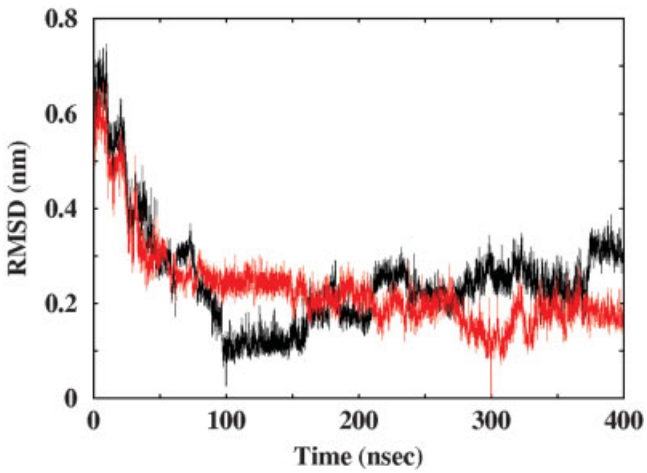


Fig. 4. The time evolution of the backbone positional RMSD of the predicted trSC3 model in aqueous solution after a least-square best fit to two reference conformations SCI (black line) and SCII (gray line) which were obtained from the simulation at 100 and 300 ns.

### SC3 Model on Air/Water Interface

As noted above, two independent simulations of 100 ns each were performed at an air/water interface, one starting from the SCI model and one from the SCII model. The SCI structure was placed in the middle of the water phase and oriented such that the loop containing residues 14–47 projected toward the interface. The minimum distance

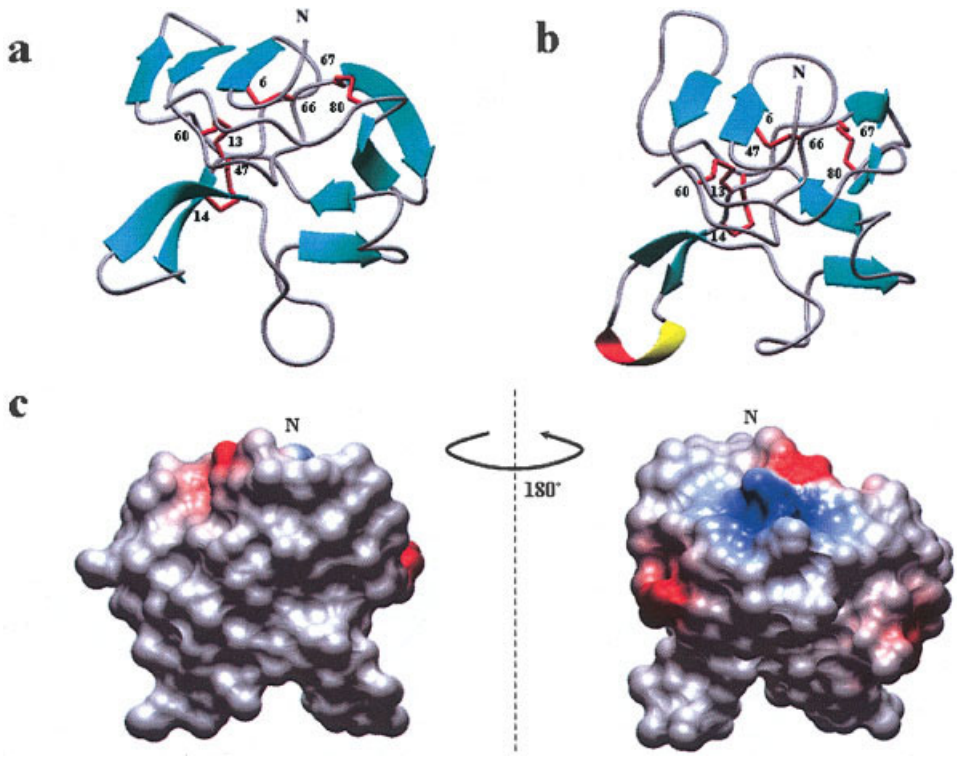


Fig. 6. **a:** One representative conformation of trSC3 model taken from the control at 100 ns (termed SCI). **b:** The other representative conformation of trSC3 model taken from the control at 300 ns (termed SCII). **c:** The electrostatic potential surface of SCI taken from two opposite directions: regions with relatively high electrostatic potential are colored red or blue whereas regions with relatively low potential are gray.

between the center of this loop (residues 20–40) and the interface is plotted as a function of simulation time in Figure 7(a). During the simulation, the structure oscillated between being completely immersed in the water phase and being partially exposed to the air phase (Fig. 8). The early stages of the simulation were characterized by a number of brief (<2 ns) binding events followed by rapid release. Later in the simulation, the protein bound to the interface for longer periods (>10 ns) via the 14–47 loop. The percentage of β-sheet remains effectively constant throughout. There is intermittent formation of helix in the loop containing residues 14–47 but no obvious correlation between the secondary structure content and whether or not the peptide was bound to the interface [Fig. 9(a)].

The simulation starting from the SCII model was also initiated with the protein in the center of the water phase. However, the model was rotated by 90° with respect to SCI so that the 14–47 loop lay parallel to the interface. Interestingly, although the conformations of SCI and SCII are very similar, their interaction with the interface was quite different. In the early stages of the simulation, the SCII structure rotated in the water phase and adsorbed strongly to the air/water interface, exposing the 14–47 loop to the air surface. As can be seen from Figure 7(b), the protein remained attached to the interface in this position during the remainder of the simulation. Adsorption was associated with a slight loss of β-structure but a marked enhancement in α-helical content in the region of the protein exposed to air [Fig. 9(b)]. Note, both SCI and SCII primarily bound to the air/water interface via the 14–47 loop.

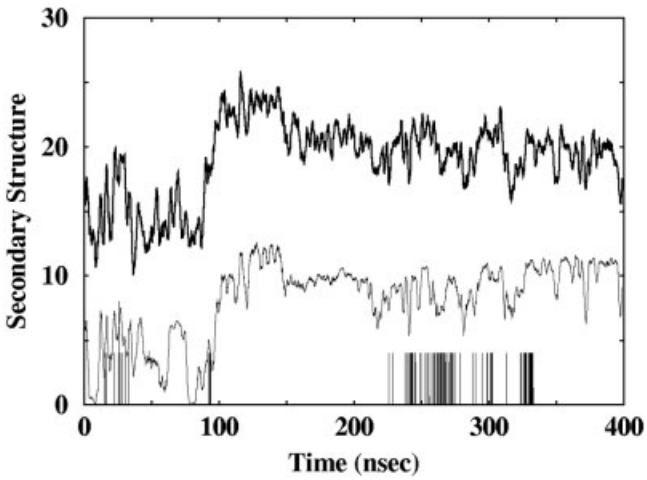


Fig. 5. The time evolution of the elements of secondary structure (numbers of residues) of the trSC3 model in the reference simulation: β-sheet in trSC3 (thick black line); β-sheet in the region between the third and fourth Cys (thin black line); α-helix in trSC3 the same as in the region between the third and fourth Cys (black intermittent line).

### SC3 Model on Oil/Water Interface

Two 100-ns simulations were performed at an oil/water interface, with again one starting from SCI and one from SCII. The setup of the two simulations was similar to that used for the air/water interface. SCI was initially placed such that the loop 14–47 was pointing toward the oil phase. The orientation of SCII was rotated by 90° with respect to SCI. During the simulations, both SCI and SCII rapidly bound to the oil/water interfaces via the 14–47 loop [Fig. 7(c, d)]. SCII reoriented on the oil surface during the early stages of binding. Both structures gradually became embedded in the dodecane phase along the simulations. Nevertheless, the terminal regions of both structures projected into the water phase. The secondary structure content is presented in Figure 9(c, d). An increase in α-helical content was only observed in the 14–47 loop and was more pronounced in the case of SCII than for SCI.

### SC3 Model on Hydrophobic Solid Surface

As in the previous simulations, SCI was orientated such that the loop of residues 14–47 was perpendicular to the

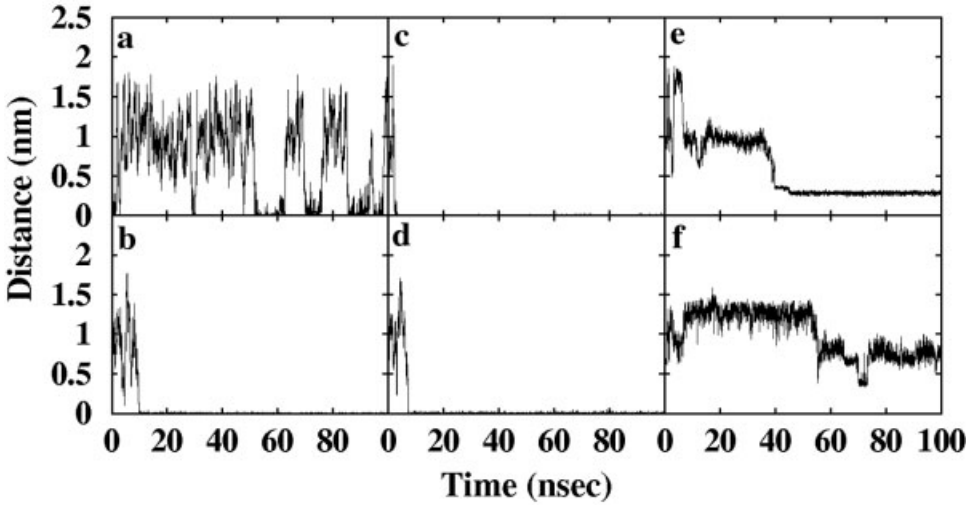


Fig. 7. The minimum distance between the center part of the 14–47 loop and a hydrophobic surface as a function of simulation time. (**a**) SCI and (**b**) SCII on an air/water interface, (**c**) SCI and (**d**) SCII on an oil/water interface, (**e**) SCI and (**f**) SCII on a hydrophobic solid/water interface.

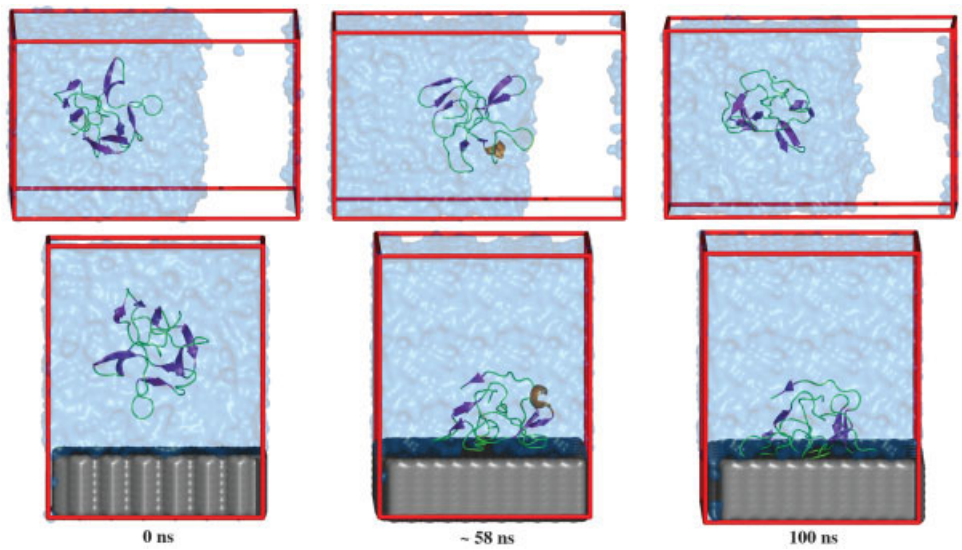


Fig. 8. **Upper graphs:** the starting conformation, conformation at about 58 ns, and the conformation at 100 ns of SCI at the air/water interface. **Lower graphs:** the starting conformation, conformation at about 58 ns, and the conformation at 100 ns of SCI at the hydrophobic solid/water interface.

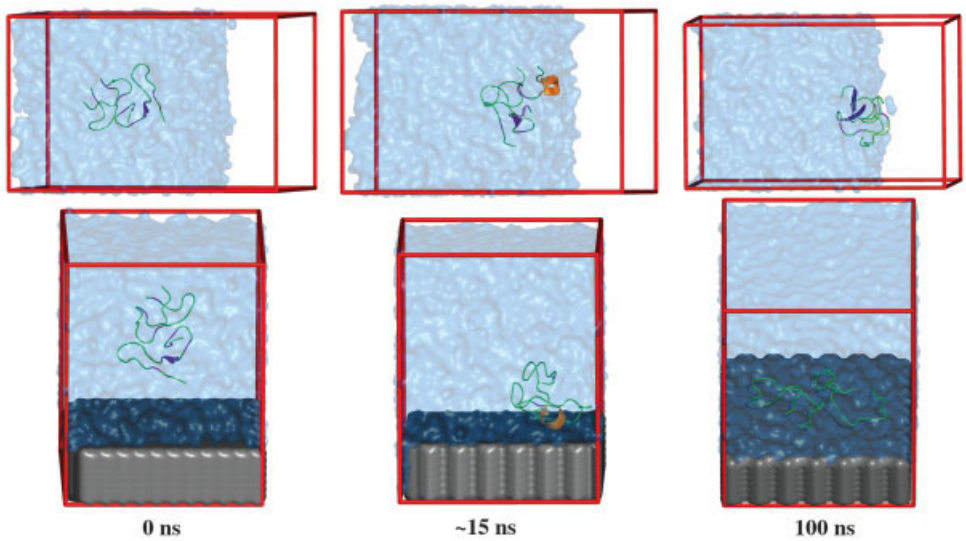


Fig. 10. **Upper graphs:** the starting conformation, conformation at about 15 ns, and the conformation at 100 ns of the dimeric peptide LPab at the air/water interface. **Lower graphs:** the starting conformation, conformation at about 15 ns, and the conformation at 100 ns of the dimeric peptide LPab at the hydrophobic solid/water interface.

surface, whereas SCII was orientated such that this loop was parallel to the interface. The minimum distance from the middle of the 14–47 loop to the solid surface is shown in Figure 7(e, f). Both SCI and SCII bind to the surface in their initial orientations and, unlike what was observed for the two fluid interfaces, the binding of trSC3 to the solid hydrophobic surface limits further motion. As SCI bound to the interface, a large region of the 14–47 loop formed direct contacts with the solid surface (Fig. 8). In contrast, a major portion of the 14–47 loop remained in solution during the binding of SCII. The number of contacts between the bound substrate and the surface was monitored in both cases. Using a cut-off of 0.6 nm, the number of contacts between SCI and the hydrophobic surface is 75% higher than that between SCII and the surface. Note, the results are insensitive to the precise value of the cut-off. The difference in the binding orientation of two trSC3 models and particularly in the involvement of the 14–47 loop, seems to correlate with differences in the adsorption to the hydrophobic surface. Interestingly, SCI and SCII also show differences in secondary structure content upon binding. In the case of SCI, the percentage of β-sheet in the molecule decreases whereas there was an increase in α-helical content in the 14–47 loop [Fig. 9(e)]. In contrast, in SCII, the 14–47 loop projects into solution. In this case, the protein attaches

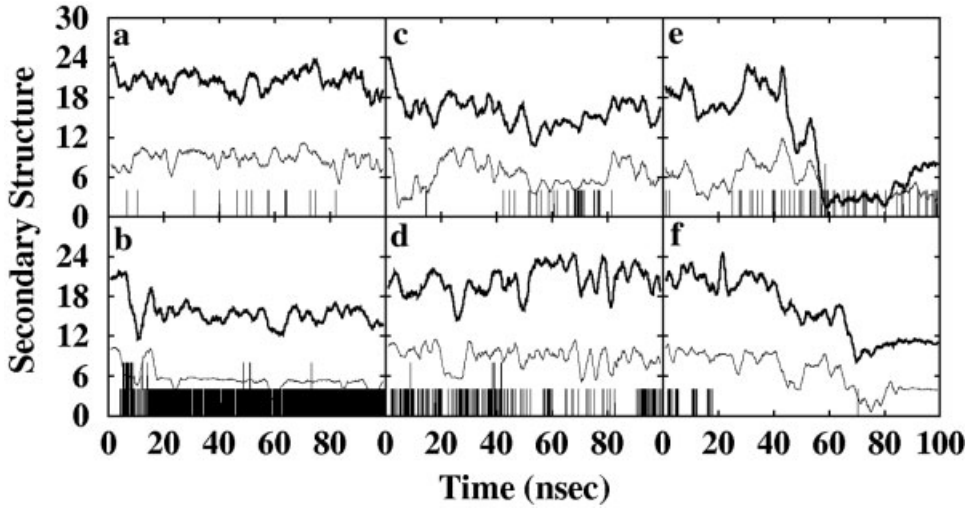


Fig. 9. The secondary structure content of the trSC3 model at the different interfaces: β-sheet in trSC3 (thick black line); β-sheet in the region between the third and fourth Cys (thin black line); α-helix in trSC3 the same as in the region between the third and fourth Cys (black intermittent line). (**a**) SCI and (**b**) SCII on an air/water interface, (**c**) SCI and (**d**) SCII on an oil/water interface, (**e**) SCI and (**f**) SCII on a hydrophobic solid/water interface.

less tightly to the surface, the percentage of β-sheet is largely preserved, and no increase in α-helical content on binding is observed [Fig. 9(f)].

### Fragment (Asn15–Ser37) of trSC3

As noted in the Introduction, a 25-residue peptide fragment from Cys13 to Ser37 corresponding to the region Cys39–Ser63 in native SC3 binds strongly to hydrophobic surfaces adopting an α-helical conformation.[27] To investigate this region in more detail, a peptide from Asn15 to Ser37 (the first two cysteine residues were excluded) was simulated in aqueous solution and at an air/water and a hydrophobic solid/water interface. One aim of this aspect of the study was to investigate possible differences between the binding of a peptide monomer and a peptide dimer to different interfaces. The region Asn15 to Ser37 is primarily hydrophobic and by analogy to HFBII is likely to be partially buried on dimerization in trSC3. In addition, when two copies of this peptide were simulated together, they rapidly dimerized suggesting that the peptide would also be a dimer in solution (see Materials and Methods).

Before investigating the behavior of the peptide at the different interfaces, control simulations were performed in water. Both peptide monomers (LPa and LPb) formed some β-sheet structure in water. As noted above, when placed together in a box, LPa and LPb rapidly (<1 ns) formed a dimer (LPa/LPb) which remained stable throughout the remainder of the simulation. The equilibrated dimer (LPab) showed an increase in β-sheet structure with respect to the monomers. α-Helix formation was observed only rarely during the simulation of dimer.

Four 100-ns simulations were performed at the two interfaces using LPa, LPb, LPa/LPb, and LPab as starting configurations. Rapid adsorption (<5 ns) to the interface was observed in most cases. At the air/water interface, both monomeric peptides (LPa, LPb) showed an increase in β-sheet content relative to the control simulations. The formation of α-helix was negligible. In contrast, both dimers showed some helix formation on binding (Fig. 10). In addition, the binding of the two alternative dimer configurations (LPa/LPb, LPab) to the air/water interface resulted in an increase in intermolecular contacts between the two monomers relative to that in solution. On the solid surface, a large decrease in β-sheet content was observed in both monomers. Similar to the behavior observed at the air/water interface, helical structure was induced in both dimers on binding. However, the number of contacts between two monomers after initially increasing on binding, decreased progressively, as the peptides absorbed further onto the hydrophobic solid surface, leading to the dissociation of the dimers.

## DISCUSSION

The most interesting feature of hydrophobins is that they are surface active and self-assemble into amphipathic membranes at hydrophobic/hydrophilic interfaces. In particular, SC3 has remarkable surface activity and forms highly insoluble, stable assemblies at interfaces. Because of its strong tendency to aggregate, the experimental determination of the three-dimensional structure of SC3 has so far not been possible. However, because SC3 is experimentally the best characterized of any of the class I or class II hydrophobins in terms of structure/function relationships, it has been possible to validate the results of the modeling and simulation studies performed in this work by comparison with a range of experimental data.

The model we propose for the structure of trSC3 in solution is compact, globular, and stabilized by a network of disulfide bridges analogous to that found in the crystal structure of class II hydrophobin HFBII.[29] Two disulfide pairs, Cys6–Cys66 and Cys13–Cys60, link the N- and C-terminal regions of the protein limiting the flexibility of

the entire molecule. The N- and C-termini and an amphiphilic β-hairpin connected by the seventh and eighth Cys are located on one face of the protein. It is expected that this side of the protein would partition toward the more hydrophilic phase. The 34-residue loop from the third to fourth cysteine (Cys14, Cys47), which is one of the primary differences between class I and II hydrophobins, is located on the other face.[4,11] In our proposed model for trSC3, this loop is exposed at the surface of the molecule. This loop is expected to be mobile and has a hydrophobic patch in the middle. It likely represents the site of primary interaction with a hydrophobic surface. The functional importance of this part is also suggested by the observation that class II hydrophobins, which have a much smaller loop between the third and fourth Cys (~11 residues) and bind less tightly to hydrophobic surfaces.[1,17,57] Simulated in aqueous solution, the protein as a whole adopted mainly β-sheet and coil conformations, nevertheless short regions of helix did appear within the 14–47 loop.

Because the sequence identity between HFBII and trSC3 is weak, the local structural details within the homology model of trSC3 are not expected to be highly accurate. However, the disulfide pattern and spacing within hydrophobins are highly conserved. It is thus very probable that trSC3 and HFBII have the same disulfide pairings and thus very likely that the trSC3 model has the correct global fold. For example, the homology model predicts that the trSC3 molecule is amphipathic. The two charged termini are located on one side of the trSC3 model whereas the hydrophobic 14–47 loop is located on the other. Interestingly, such amphipathic character was recently shown experimentally by Joel Mackay and coworkers in regard to another class I hydrophobin, EAS.

Based on the proposed homology model of trSC3, the surface activity of this protein was examined by simulating the protein monomer at an air/water, an oil/water, and a hydrophobic solid/water interface. Two alternative configurations of trSC3, with similar overall folds, were selected from different stages of a simulation in water. These two structures were placed in different orientations with respect to the interface and simulated independently.

In general, both models of the protein attached rapidly to the different hydrophobic surfaces. At the air/water and oil/water interfaces, further structural rearrangements are observed after binding. This correlates well with the experimental observation that, at such interfaces, the intermediate α-helical state is only short-lived. A stable β-sheet state forms within minutes.[25,26] Both of the trSC3 models tended to adsorb to the different interfaces via the 14–47 loop. The protein bound most strongly to the solid surface, with the protein becoming immobilized upon binding. The number of contacts between the protein and the solid surface were greatest when the 14–47 loop participated in binding. This again suggests an important role for this loop in binding. We also note that α-helical structure was only ever observed in the 14–47 loop. During the adsorption of the protein to the three interfaces, an increase in the α-helix content in this loop with respect to that in the control simulation was observed, but only when this loop was involved in the attachment to the surfaces. This is again consistent with experimental data suggesting that the 14–47 loop is responsible for the α-helical structure formation and is involved in the subsequent formation of the β-sheet state on both an air and an oil surface.[27]

Hydrophobin SC3 is believed to be primarily dimeric in solution.[23] Dimeric SC3 has also been suggested to be the primary building unit for both aggregation in solution and self-assembly at hydrophobic/hydrophilic interfaces.[23] However, when bound to Teflon, FRET is not observed. This suggests that SC3 is essentially monomeric on such surfaces.[22] To address the question of whether binding might initially occur as a monomer or dimer, simulations were performed of a portion of the loop between the third and fourth Cys in solution, at an air/water and a hydrophobic solid/water interface. This region of the protein is believed to be critical to both dimer formation and binding to hydrophobic/hydrophilic interfaces. It was shown that when dimers of this peptide were allowed to bind to a solid surface, the dimers dissociated.

Note, the model of trSC3, a class I hydrophobin, was predicted from the X-ray structure of HFBII, a class II hydrophobin. The current study assumes that the disulfide pairings are identical in both classes of hydrophobins. Another limitation to this work is that the simulations can only probe events on timescales of hundreds of nanoseconds. In addition, approximations were made in the construction of the hydrophobic surface. This does not correspond exactly to a specific set of experimental conditions. Despite these uncertainties, the current study yields qualitative agreements with a range of experimental observations. In particular, we show that the α-helical state of trSC3 can be induced in the early stages of adsorption on hydrophobic/hydrophilic interfaces. We also show that the substrate may preferentially attach to a hydrophobic surface via the loop region between the third and fourth Cys and that this region is critical for the formation of the α-helical state. Studies on this specific peptide fragment not only offered further evidence for surface activity of this region of the protein, but also indirectly supported the suggestion that dimeric SC3 dissociates on Teflon surface.

Combining what is known in regard to SC3 to date, it is reasonable to propose that the adsorption of SC3 onto hydrophobic solid surface involves the following steps: 1) SC3 (or trSC3) likely exists as dimer in solution with the hydrophobic patch in the loop between Cys14 and Cys47 being largely buried at the dimer interface; 2) SC3 would first bind to a hydrophobic solid surface as a dimer and then dissociate; 3) the separated monomers attach tightly to the surface and adopt the α-helical state; and 4) the subsequent assembly of the monomers into the final rodlet state, experimentally a very slow process, would thus depend on the diffusion and aggregation of individual monomers.

## ACKNOWLEDGMENTS

The authors thank Professor Barry Honig for help in the structure prediction of trSC3 and Professor Joel P. Mackay for sharing results on hydrophobin EAS before publication. The authors are also grateful to Dr. Ronen Zangi for useful discussions and Drs. Alex de Vries and Tsjerk Wassenaar for help in constructing the interfaces.

## REFERENCES

1. Wessels JGH. Hydrophobins: proteins that change the nature of the fungal surface. Adv Microb Physiol 1997;38:1–45.
2. Wösten HAB, Wessels JGH. Hydrophobins, from molecular structure to multiple functions in fungal development. Mycoscience 1997;38:363–374.
3. Wösten HAB, van Wetter MA, Lugones LG, van der Mei HC, Busscher HJ, Wessels JGH. How a fungus escapes the water to grow into the air. Curr Biol 1999;9:85–88.
4. Wösten HAB, de Vries OMH, Wessels JGH. Interfacial self-assembly of a fungal hydrophobin into a hydrophobic rodlet layer. Plant Cell 1993;5:1567–1574.
5. Wösten HAB, Ruardy TG, van der Mei HC, Busscher HJ, Wessels JGH. Interfacial self-assembly of a *Schizophyllum commune* hydrophobin into an insoluble amphipathic membrane depends on surface hydrophobicity. Colloids Surf B Biointerfaces 1995;5:189–195.
6. Wösten HAB, Schuren FHJ, Wessels JGH. Interfacial self-assembly of a hydrophobin into an amphipathic protein membrane mediates fungal attachment to hydrophobic surface. EMBO J 1994;13:5848–5854.
7. Russo PS, Blum FD, Ipsen JD, Miller WG, Abul-Hajj YJ. The surface activity of the phytotoxin cerato-ulmin. Can J Bot 1982;60: 1414–1422.
8. Lugones LG, Bosscher JS, Scholtmeijer K, de Vries OMH, Wessels JGH. An abundant hydrophobin (ABH1) forms hydrophobic rodlet layers in *Agaricus bisporus* fruiting bodies. Microbiology 1996;142: 1321–1329.
9. Lugones LG, Wösten HAB, Birkenkamp KU, Sjollema KA, Zagers J, Wessels JGH. Hydrophobins line air channels in fruiting bodies of *Schizophyllum commune* and *Agaricus bisporus*. Mycol Res 1999;103:635–640.
10. Lugones LG, Wösten HAB, Wessels JGH. A hydrophobin (ABH3) specifically secreted by vegetatively growing hyphae of *Agaricus bisporus* (common white button mushroom). Microbiology 1998; 144:2345–2353.
11. Scholtmeijer K, Wessels JGH, Wösten HAB. Fungal hydrophobins in medical and technical applications. Appl Microbiol Biotechnol 2001;56:1–8.
12. Janssen MI, van Leeuwen MBM, Scholtmeijer K, van Kooten TG, Dijkhuizen L, Wösten HAB. Coating with genetic engineered hydrophobin promotes growth of fibroblasts on a hydrophobic solid. Biomaterials 2002;23:4847–4854.
13. Scholtmeijer K, Janssen MI, Gerssen B, et al. Surface modifications created by using engineered hydrophobins. Appl Environ Microbiol 2002;68:1367–1373.
14. Nakari-Setala T, Azeredo J, Henriques M, et al. Expression of a fungal hydrophobin in the *Saccharomyces cerevisiae* cell wall: effect on cell surface properties and immobilization. Appl Environ Microbiol 2002;68:3385–3391.
15. Palomo JM, Penas MM, Fernandez LG, et al. Solid-phase handling of hydrophobins: immobilized hydrophobins as a new tool to study lipases. Biomacromolecules 2003;4:204–210.
16. Bilewicz R, Witomski J, van der Heyden A, Tagu D, Palin B, Rogalska E. Modification of electrodes with self-assembled hydrophobin layers. J Phys Chem B 2001;105:9772–9777.
17. Wessels JGH. Developmental regulation of fungal cell wall formation. Annu Rev Phytopathol 1994;32:413–437.
18. Yaguchi M, Pusztai-Carey M, Roy C, et al. Amino acid sequence and spectroscopic studies of Dutch Elm disease toxin, cerato-ulmin. In: Sticklen MB, Sherald JL, editors. Dutch elm disease research, cellular and molecular approaches. New York: Springer-Verlag; 1993. p 152–170.
19. de Vries OMH, Fekkes MP, Wösten HAB, Wessels JGH. Insoluble hydrophobin complexes in the walls of *Schizophyllum commune* and other filamentous fungi. Arch Microbiol 1993;159:330–335.
20. Wessels JGH, de Vries OMH, Asgeirsdottir SA, Schuren FHJ. Hydrophobin genes involved in formation of aerial hyphae and fruit bodies in *Schizophyllum commune*. Plant Cell 1991;3:793–799.
21. Carpenter CE, Mueller RJ, Kazmierczak P, Zhang L, Villalon DK, van Alfen NK. Effect of a virus on accumulation of a tissue-specific cell-surface protein of the fungus Cryphonectria (Endothia) parasitica. Mol Plant Microbe Interact 1992;4:55–61.
22. Wang X, de Vocht ML, de Jonge J, Poolman B, Robillard GT. Structure changes and molecular interactions of hydrophobin SC3 in solution and on a hydrophobic surface. Protein Sci 2002;11:1172–1181.
23. Wang X, Graveland-Bikker JF, de Kruif CG, Robillard GT. Oligomerization of hydrophobin SC3 in solution: from soluble state to self-assembly. Protein Sci 2004;13:810–821.
24. de Vocht ML, Scholtmeijer K, van der Vegte EW, et al. Structural characterization of the hydrophobin SC3, as a monomer and after self-assembly at hydrophobic/hydrophilic interfaces. Biophys J 1998;74:2059–2068.
25. de Vocht ML, Reviakine I, Ulrich WP, et al. Self-assembly of the hydrophobin SC3 proceeds via two structural intermediates. Protein Sci 2002;11:1199–1205.
26. Wang X, Shi F, Wösten HAB, Hektor H, Poolman B, Robillard GT. The SC3 hydrophobin self-assembly into a membrane with distinct mass transfer properties. Biophys J 2005;88:3434–3443.
27. Wang X, Permentier HP, Rink R, et al. Probing the self-assembly and the accompanying structural changes of hydrophobin SC3 on a hydrophobic surface by mass spectrometry. Biophys J 2004;87: 1919–1928.
28. Zangi R, de Vocht ML, Robillard GT, Mark AE. Molecular dynamics study of the folding of hydrophobin SC3 at a hydrophilic/hydrophobic interface. Biophys J 2002;83:112–124.
29. Hakanpää J, Paananen A, Askolin S, et al. Atomic resolution structure of the HFBII hydrophobin, a self-assembling amphiphile. J Biol Chem 2004;279:534–539.
30. Zhou H, Zhou Y. Single-body residue-level knowledge-based energy score combined with sequence-profile and secondary structure information for fold recognition. Proteins 2004;55:1005–1013.
31. Petrey D, Xiang X, Tang CL, et al. Using multiple structure alignments, fast model building, and energetic analysis in fold recognition and homology modeling. Proteins 2003;53:430–435.
32. Ponder JW. Tinker software tool for molecular design, Version 3.7. Washington University; 1999.
33. Jorgensen WL, Maxwell DS, Tirado-Rives J. Development and testing of the OPLS all-atom force field on conformational energetics and properties of organic liquids. J Am Chem Soc 1996;118: 11225–11236.
34. Jorgensen WL, McDonald NA. Development of an all-atom force field for heterocycles. Properties of liquid pyridine and diazenes. J Mol Struct (THEOCHEM) 1998;424:145–155.
35. McDonald NA, Jorgensen WL. Development of an all-atom force field for heterocycles. Properties of liquid pyrrole, furan, diazoles, and oxazoles. J Phys Chem B 1998;102:8049–8059.
36. Price MLP, Ostrovsky D, Jorgensen WL. Gas-phase and liquid-state properties of esters, nitriles, and nitro compounds with the OPLS-AA force field. J Comput Chem 2001;22:1340–1352.
37. Jorgensen WL, Tirado-Rives J. The OPLS potential functions for proteins: energy minimizations for crystals of cyclic peptides and crambin. J Am Chem Soc 1998;110:1657–1666.
38. Gallicchio E, Levy RM. AGBNP: an analytic implicit solvent model suitable for molecular dynamics simulations and high-resolution modeling. J Comput Chem 2004;25:479–499.
39. Fan H, Mark AE, Zhu J, Honig B. Comparative study of generalized Born models: protein dynamics. Proc Natl Acad Sci USA 2005;102:6760–6764.
40. Nocendal J, Wright SJ. Numerical optimization. New York: Springer; 1999. p 224–226.
41. Berendsen HJC, van der Spoel D, van Drunen R. GROMACS: a message-passing parallel molecular dynamics implementation. Comput Phys Commun 1995;91:43–56.
42. Lindahl E, Hess B, van der Spoel D. GROMACS 3.0: a package for molecular simulation and trajectory analysis. J Mol Modeling 2001;7:306–317.
43. van der Spoel D, van Buuren AR, Apol E, et al. Gromacs user manual, Version 3.0. Nijenborgh 4, 9747 AG Groningen, the Netherlands; 2001. Available at: http://www.gromacs.org.
44. van Gunsteren WF, Billeter SR, Eising AA, et al. Biomolecular

simulation: the GROMOS96 manual and user guide. vdf Hochschulverlag AG, Zürich; 1996.
45. Schuler LD, van Gunsteren WF. On the choice of dihedral angle potential energy functions for n-alkanes. Mol Simul 2000;25:301–319.
46. Tironi IG, Sperb R, Smith PE, van Gunsteren WF. A generalized reaction field method for molecular dynamics simulations. J Chem Phys 1995;102:5451–5459.
47. Feenstra KA, Hess B, Berendsen HJC. Improving efficiency of large time-scale molecular dynamics simulations of hydrogen-rich systems. J Comput Chem 1999;20:786–798.
48. Hess B, Bekker H, Berendsen HJC, Fraaije JGEM. LINCS: a linear constraint solver for molecular simulations. J Comput Chem 1997;18:1463–1472.
49. Miyamoto S, Kollman PA. SETTLE: an analytical version of the SHAKE and RATTLE algorithm for rigid water models. J Comput Chem 1992;13:952–962.
50. Berendsen HJC, Postma JPM, van Gunsteren WF, Hermans J. Interaction models for water in relation to protein hydration. In: Pullman B, editor. Intermolecular forces. Dordrecht, the Netherlands: Reidel; 1981. p 331–342.
51. Berendsen HJC, Postma JPM, van Gunsteren WF, Di Nola A, Haak JR. Molecular dynamics with coupling to an external bath. J Chem Phys 1984;81:3684–3690.
52. Kabsch W, Sander C. Dictionary of protein secondary structure: pattern recognition of hydrogen-bonded and geometrical features. Biopolymers 1983;22:2577–2637.
53. McGuffin LJ, Bryson K, Jones DT. The PSIPRED protein structure prediction server. Bioinformatics 2000;16:404–405.
54. Jones DT. Protein secondary structure prediction based on position-specific scoring matrices. J Mol Biol 1999;292:195–202.
55. Koradi R, Billeter M, Wüthrich K. MOLMOL: a program for display and analysis of macromolecular structures. J Mol Graphics 1996;14:51–55.
56. Richards FM. Areas, volumes, packing and protein structure. Annu Rev Biophys Bioeng 1977;6:151–176.
57. Wösten HAB. Hydrophobins: multipurpose proteins. Annu Rev Microbiol 2001;55:625–646.